Proceedings of the ASME 2024
International Design Engineering Technical Conferences and
Computers and Information in Engineering Conference
IDETC-CIE2024
August 25-28, 2024, Washington, DC

DETC2024-143590

EXPERIMENTAL STUDY ON DYNAMIC CHARACTERISTICS OF A TENSEGRITY STRUCTURE USING A 3D SLDV SYSTEM

Ke Yuan [1], Sichen Yuan [2], Weidong Zhu [1,*]

[1]Department of Mechanical Engineering, University of Maryland, Baltimore County, 1000 Hilltop Circle, Baltimore, 21250, MD, USA
[2]Department of Aerospace Engineering and Mechanics, University of Alabama, 251 Shelby Lane, Tuscaloosa, 35487, AL, USA

ABSTRACT

Tensegrity structures have emerged as important components of various engineering structures due to their high stiffness, light weight, and deployable capability. Existing studies on dynamic analyses of tensegrity structures mainly focus on responses of their nodal points while overlook deformations of their cable and strut members. This study aims to propose a non-contact approach for experimental modal analysis of a tensegrity structure to identify its three-dimensional (3D) natural frequencies and full-field mode shapes, which include modes with deformations of its cable and strut members. A 3D scanning laser Doppler vibrometer (SLDV) is used with a mirror for extending its field of view to measure full-field vibration of a three-strut tensegrity column with free boundaries. Tensions and axial stiffnesses of cable members of the tensegrity column are determined using natural frequencies of their transverse and longitudinal modes, respectively, and used to build a numerical model of the tensegrity column for dynamic analysis and model validation purposes. Modal assurance criterion (MAC) values between experimental and numerical mode shapes are used to identify their paired modes. Natural frequencies and mode shapes of the first 15 elastic modes of the tensegrity column are identified from the experiment, which include modes of the overall structure and its cable members. These identified modes can be classified into five mode groups depending on their types. Five modes are paired between experimental and numerical results with MAC values larger than 78%. Differences between natural frequencies of paired modes of the tensegrity column are less than 15%. The non-contact 3D vibration measurement approach presented in this work can measure responses of nodal points, as well as deformations of cable and strut members, of the tensegrity column, and allows accurate estimation of its 3D full-field modal parameters.

Keywords: Tensegrity structure, 3D SLDV with a mirror, modal analysis, 3D full-field vibration measurement, model validation

1. INTRODUCTION

Tensegrity structures are a type of structures that consist of only cable and strut members and can be in self-equilibrium and free-standing without any external support [1]. They have been widely used as elements of various engineering structures, such as pedestrian bridges [2], membrane roof skeletons [3], and nanoscale structures [4], due to their optimized shape, high stiffness, and light weight. They can also be used in soft robots [5, 6] and satellite reflectors [7–9] due to their deployable capability.

Many studies focused on form-finding of a tensegrity structure [10], which was the key and first step to build its accurate numerical or analytical model. Tibert and Pellegrino [11] reviewed seven commonly used form-finding methods for tensegrity structures and classified them as kinematic and static methods. It was reported that kinematic methods were suitable for tensegrity structures with well-known configuration details, while the force density method, which was one of the static methods, was suitable for searching for new configurations of tensegrity structures. For the form-finding problem of a large-scale tensegrity structure, the calculation efficiency became a major concern. Koohestani [12] proposed an efficient form-finding method using a genetic algorithm, which was validated by various symmetrical tensegrity structures. Recently, Yuan and Zhu [13] proposed a stochastic fixed nodal position method by combining a fixed nodal position method [14] and a stochastic optimization algorithm [15]. This method was applicable for form-finding of a large-scale and geometrically irregular tensegrity structure. With an accurate numerical or analytical model of a tensegrity structure, a static analysis aiming to evaluate its rigidity and stability, as well as a dynamic analysis aiming to obtain its dynamic characteristics, can be conducted. Guest [16] investigated relations between the stiffness of a tensegrity structure and its connectivity, geometry, material properties, and prestress using its analytical model. Kan et al. [17] conducted static and dynamic analyses of a two-strut collision model of a tensegrity structure to address its strut

*Corresponding author: wzhu@umbc.edu
Documentation for `asmeconf.cls`: Version 1.37, May 27, 2024.

collision problem. Ma et al. [18] developed a finite element (FE) method that was denoted as TsgFEM using the Lagrangian method with nodal coordinate vectors considered as generalized coordinates to conduct dynamic analyses on tensegrity structures. Another important application related to tensegrity structure dynamics is tensegrity feedback control [19–21]. Linear and nonlinear dynamics of a tensegrity system, such as a tensegrity robotic reacher and a tensegrity-membrane system, can be used to design its controller.

There are still insufficient investigations on 1) the dynamic analysis of an entire tensegrity structure, incorporating responses of its nodal points as well as deformations of its cable and strut members, and 2) comparison and validation between experimental and numerical modal analyses of the entire tensegrity structure. The first research gap is due to oversimplification of dynamic models of tensegrity structures in traditional modeling methods, such as the Lagrange method [22] and the FE method [23], where internal displacements of cable and strut members are usually ignored. In Refs. [24, 25], numerical modeling problems of tensegrity-membrane systems were systematically investigated. A shell-beam-cable model, a membrane-truss-cable model and a control-oriented model were developed to obtain dynamic responses of structural members of a tensegrity-membrane system including its membrane, bars, and tendons, as well as those of the entire system. Yuan and Zhu [26] developed a numerical method, which was referred to as the Cartesian spatial discretization (CSD) method, to incorporate internal displacements of structural members, comprising both cables and struts, of a tensegrity structure in its dynamic modeling. Incorporation of member internal displacements grants the CSD method an ability to provide accurate results for vibration analysis of the entire tensegrity structure. In addition, use of the global Cartesian coordinate system in the CSD method provides a fast and straight-forward assembly of equations of motion when deriving them for the entire tensegrity structure. However, dynamic responses of the tensegrity structure calculated by the CSD method have not been compared to those from the experiment, which constitutes the second research gap. The major reason for the second research gap is that previous studies on experimental modal analysis of a tensegrity structure used accelerometers to measure its responses. As a type of contact sensors, while an accelerometer can be attached to nodal points of a tensegrity structure to obtain their responses, it was not suitable for measuring vibrations of cable members of the tensegrity structure due to the mass-loading problem. For instance, Bossens et al. [27] conducted modal analysis of a three-stage tensegrity structure using single-axis accelerometers to acquire its response data at its nodal points. Without knowing exact properties and pretensions of cable members, they conducted model updating on a FE model of the tensegrity structure based on its experimental modal parameters. It was reported that the first two bending and torsional modes from the updated FE model matched those obtained from the experiment in the frequency domain. Małyszko and Rutkiewicz [28] conducted modal analysis of a single-stage tensegrity simplex using a modal hammer and triaxial accelerometers attached to its nodal points. Prestresses of cable members were adjusted to different levels and measured by build-in force transducers, and the effect of the prestress level on natural frequencies of the tensegrity simplex was investigated using both experimental and FE methods. In both studies, only overall mode shapes of the tensegrity structure were identified using accelerometers.

To address research gaps mentioned above, this work first proposed a non-contact vibration measurement method for obtaining three-dimensional (3D) full-field modal parameters of a tensegrity column. A 3D scanning laser Doppler vibrometer (SLDV) was used along with a mirror to obtain 3D vibrations all of its nodal points and cable and strut members to identify its natural frequencies and full-field mode shapes. Unlike an accelerometer, a laser vibrometer can avoid the mass-loading problem via a non-contact way [29, 30], which is essential for structures like a tensegrity column since mass-loading can significantly affect its dynamic response. Although the laser vibrometer has been widely used in modal parameter estimation [31, 32] and structural damage detection [33],its field of view (FOV) can be limiting when measuring the tensegrity column with a complex spatial shape. A mirror was used in this work to extend the FOV of the 3D SLDV, enabling its laser beams to reach areas beyond its FOV. Natural frequencies and mode shapes of the first 15 elastic modes of the tensegrity column are identified from the experiment, which include modes of the overall structure and its cable members. These identified modes can be classified into five mode groups depending on their types. Modal assurance criterion (MAC) values among experimental mode shapes that are referred to as AutoMAC show that obtaining 3D vibrations and mode shapes of a structure with a complex 3D shape, such as the tensegrity column in this work, is significant for distinguishing its modes, which can be indistinguishable from its one-dimensional (1D) vibration and mode shapes. A cable clamping device was designed and used with the 3D SLDV to measure transverse and longitudinal vibrations of cable members for determining accurate cable tensions and axial stiffnesses, respectively. A form-finding method referred to as the force density method with member grouping was used to build a numerical model of the tensegrity column with initial parameters, including cable tensions and axial stiffnesses, which are obtained from vibration-based measurements. The CSD method, which avoids the oversimplification problem in traditional methods for dynamic analyses of tensegrity structures, is used to obtain modal parameters of the tensegrity column. MAC values between experimental and numerical mode shapes are used to identify their paired modes. Five modes are paired between experimental and numerical results with MAC values larger than 78%. Differences between natural frequencies of paired modes of the tensegrity column are less than 15%.

The remainder of this paper is organized as follows. Design considerations of a strut-cable interface of a three-strut tensegrity column are discussed in Section 2 to address construction and robustness issues. Dimensions of the final assembled tensegrity column are presented there. Experimental modal analysis of the tensegrity column, including details of the experimental setup and modal parameter estimation are presented in Section 3. Methods for building the numerical model of the tensegrity column using results from vibration measurements, and numerical modal analysis using the CSD method are proposed in Section

4. This section also includes comparison between experimental and numerical modal parameters, followed by some discussions. Section 5 presents some conclusions.

2. DESIGN AND ASSEMBLY OF THE THREE-STRUT TENSEGRITY COLUMN

The test structure in this work is a typical three-strut tensegrity column as shown in Fig. 1. It is selected as the analyzed structure in this work as it is a basic type of tensegrity structures and suitable for validation of the experimental modal analysis method proposed in this work. It consists of three strut members, represented by black solid lines in Fig. 1a, in compression, and nine cable members, represented by red dashed lines, in tension. The tensegrity column has two equilateral triangular bases formed by six horizontal cables. Their six vertices are connected by three vertical cables along with three struts, resulting in six nodal points of the tensegrity column. In this work, a cable or strut member is denoted by nodal numbers of its two ends; for instance the cable 2_6 and the strut 1_5. Two design rules for a reasonable strut-cable interface of a tensegrity structure, addressing construction and robustness issues, were proposed in Ref. [27]:

(I) Lengths and tensions of cables attached to the interface should be adjustable to achieve the desired stiffness of the overall structure; and

(II) Cables attached to the strut-cable interface should be easily replaceable in case of breakage due to overloading during testing.

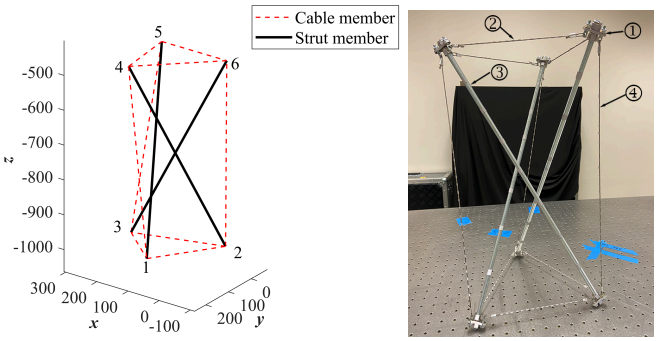

FIGURE 1: (a) Concept of the three-strut tensegrity column, consisting of three strut members represented by black solid lines in compression, and nine cable members represented by red dashed lines in tension, and (b) the actual constructed tensegrity column used as the test structure in this work

2.1 Design considerations of the tensegrity column

A mounting plate with three small holes and one large hole, as shown in Fig. 2a, was designed to mount cable and strut members at nodal points to form the strut-cable interface in this work. The mounting plate had an optimized triangular shape to reduce its size and weight, and a thickness of 0.125 inches (3.18 mm). The strut member was screwed onto the mounting plate via a nylon-insert lock nut to avoid slacking, as shown in Fig. 2b, and cable members were attached to the mounting plate via cable crimps and machine screw hangers, as shown in Fig. 2c. Cable members were locked by crimps at their ends to achieve the desired length, and screw hangers could be tightened or loosened to achieve desired tensions of cable members, following rule (I). A failed cable member could be easily replaced by cutting it at its ends and installing a new cable. Therefore, replacement of the cable member would not affect the strut member in the strut-cable interface since they were assembled through mounting plates rather than being directly interfaced, aligning with rule (II).

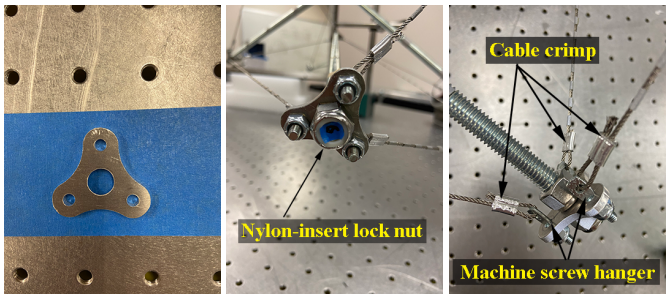

FIGURE 2: (a) Mounting plate designed for assembling cable and strut members at nodal points to form the strut-cable interface of the three-strut tensegrity column in this work, and (b) and (c) details of the strut-cable interface

2.2 Components used to assemble the tensegrity column

The assembled tensegrity column, following design considerations discussed in the previous section, is shown in Fig. 1b. Components of the tensegrity column are marked by indices, and their descriptions and numbers are detailed in Table 1. In this work, stainless-steel threaded rods with a diameter of 3/8 inches (9.53 mm) are used as strut members, and stainless-steel aircraft wires with a diameter of 1/16 inches (1.59 mm) are used as cable members. The height of the final assembled tensegrity column is 21.1 inches (535.94 mm). Lengths of its cable and strut members can be found in Table 2, with member numbers corresponding to numbers shown in Fig. 1a. Note that the vertical cable 3_5 is slightly longer than the other two vertical cables, 1_4 and 2_6, due to some assembly error. One can also see that lengths of horizontal cables vary in the range from 8.8 inches (223.52 mm) to 9.14 inches (232.16 mm) due to the same reason.

3. EXPERIMENTAL MODAL ANALYSIS OF THE THREE-STRUT TENSEGRITY COLUMN

3.1 Experimental setup

In this work, a Polytec PSV-500-3D SLDV was used to measure vibration of the tensegrity column and obtain its natural frequencies and mode shapes. The experimental setup for modal analysis of the tensegrity column is shown in Fig. 3. Non-contact measurement using the 3D SLDV can obtain not only responses of nodal points of the tensegrity column but also deformations of its cable and strut members, which was not available in previous studies using accelerometers. Two strings were used to

TABLE 1: Descriptions and numbers of components used to assemble the tensegrity column

Index	Description	Number
1	Mounting plates and nylon-insert locks used as nodal points	6
2	Stainless-steel aircraft wires with a diameter of 1/16 inches used as horizontal cables	6
3	Stainless-steel threaded rods with a diameter of 3/8 inches used as struts	3
4	Stainless-steel aircraft wires with a diameter of 1/16 inches used as vertical cables	3

TABLE 2: Lengths of cable and strut members of the final assembled tensegrity column

Member No.	Length (inch/mm)	Member No.	Length (inch/mm)
Strut 1_5	24.00/609.60	Cable 1_2	8.88/225.55
Strut 2_4	24.00/609.60	Cable 2_3	9.14/232.16
Strut 3_6	24.00/609.60	Cable 1_3	9.09/230.89
Cable 1_4	19.06/484.12	Cable 4_6	9.09/230.89
Cable 3_5	19.50/495.30	Cable 5_6	8.99/228.35
Cable 2_6	19.13/485.90	Cable 4_5	8.80/223.52

suspend the tensegrity column from a stable frame at its nodal points 1 and 4, respectively, simulating its free boundary conditions. A Labworks ET-126B shaker was attached to the nodal point 3 through a stinger to excite the tensegrity column, and a periodic chirp with a frequency bandwidth of 1000 Hz was used as the excitation source for the experiment. Small pieces of retro-reflective tapes were attached at multiple positions on surfaces of nodal points as well as those of cable and strut members to enhance signal-to-noise ratios of measured responses by the 3D SLDV. Based on the stand-off distance between the 3D SLDV and the tensegrity column during measurement, the diameter of the laser spot was about 0.02 inches (0.51 mm), which was much smaller than that of cable members (0.625 inches or 15.88 mm). This ensured that laser spots of the 3D SLDV could be precisely focused on surfaces of cable members to capture their vibrations.

As an optical-based vibration measurement device, the 3D SLDV can be limited by its FOV, especially when measuring a 3D spatial structure like the tensegrity column in this work. The 3D SLDV was fixed at one position in the experiment, with its laser beams approximately perpendicular to the cable 2_6 as shown in Fig. 3, to avoid potential errors arising from system movements. Therefore, cables 2_5, 5_6, and 2_3 were outside the FOV of the 3D SLDV. To measure their vibrations, a mirror was used to extend the FOV of the 3D SLDV [34, 35]. In Fig. 3, laser spots of the 3D SLDV could reach cables 4_5 and 5_6 when the mirror was placed at the position 1, and the cable 2_3 when at the position 2. The schematic of vibration measurement with the assistance of the mirror for areas outside the FOV of the 3D SLDV is shown in Fig. 4a. The first step of the experiment was system calibration. A reference object shown in Fig. 3 was used to calibrate the 3D SLDV and establish a global coordinate system for the tensegrity column. Another goal of calibration was to ensure that three laser spots could be focused at the same position for each measurement point, allowing acquisition of coordinates of measurement points in the FOV of the 3D SLDV. The second step was to obtain coordinates of three points on the mirror to define its plane. Coordinates of actual points on target cables and their corresponding virtual points behind the mirror could be determined. Finally, three laser spots could be focused at same positions for measurement points on cables outside the FOV of the 3D SLDV to obtain their vibrations.

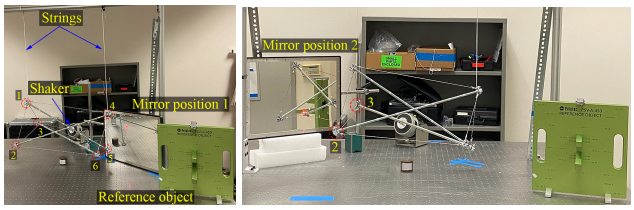

(a) (b)

FIGURE 3: Experimental setup for modal analysis of the tensegrity column, where (a) the position 1 corresponds to measurement of cables 4_5 and 5_6, and (b) the position 2 corresponds to measurement of the cable 2_3

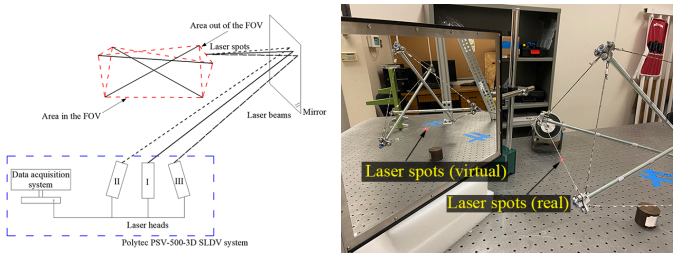

(a) (b)

FIGURE 4: (a) Schematic of vibration measurement with the assistance of the mirror on areas outside the FOV of the 3D SLDV, and (b) actual and virtual laser spots on the cable 2_3 corresponding to measurement with the mirror at the position 2

3.2 Modal parameter estimation of the tensegrity column

A total of 155 measurement points are assigned to the entire tensegrity column. Distribution of these points and their numbers are shown in Fig. 5, where blue rectangular markers represent points at nodal points, black triangular markers represent points on strut members, and red circular markers represent points on cable members. More measurement points are assigned to cable members than to strut members, since struts, owing to their much higher stiffness, can be considered as rigid bodies in the experiment. A frequency-domain analysis is conducted on responses of all measurement points on the tensegrity column to obtain the average frequency response function (FRF), a peak-picking method was used to identify its natural frequencies from the FRF, and experimental modal analysis was conducted to obtain its mode shapes [36].

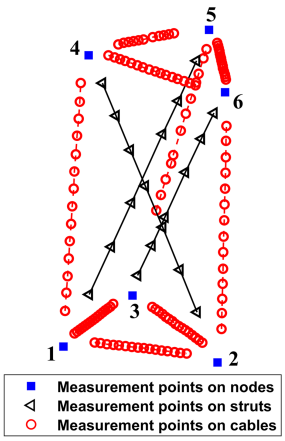

Iterms	Numbers
Strut 2_4	7-13
Cable 2_6	14-27
Strut 3_6	28-33
Strut 1_5	34-39
Cable 1_4	40-53
Cable 3_5	54-65
Cable 4_6	66-81
Cable 4_5	82-92
Cable 5_6	93-107
Cable 1_2	108-123
Cable 2_3	124-139
Cable 1_3	140-155

FIGURE 5: Distribution of measurement points on the tensegrity column, where blue rectangular markers represent points at nodal points, black triangular markers represent points on strut members, and red circular markers represent points on cable members

The log-log plot of the average FRF of all measurement points on the tensegrity column is shown in Fig. 6. The first 15 elastic modes are identified and classified into five groups based on their mode types, and marked by boxes in red dashed lines. Selected examples representing each group, along with their mode descriptions, are shown in Fig 7. The mode group 1 includes the 1st torsional mode of the tensegrity column, which is also its 1st elastic mode. In this mode, triangular planes formed by nodal points 1 through 3 and nodal points 4 through 6 rotate in opposite directions, while cable and strut members maintain a rigid-body status, resulting in torsional motion. The identified natural frequency of the highest rigid-body mode of the tensegrity column is 0.63 Hz, which is approximately 6.7% of its 1st elastic mode frequency. Therefore, simulated boundary conditions using strings, as shown in Fig. 3, can be considered as free boundary conditions, as the frequency ratio is less than 10%, as proposed by Ref. [36]. Modes 2 through 15 are pure cable modes without nodal motions. The mode group 2 includes the 2nd through 4th modes of the tensegrity column, which are the 1st bending modes of its vertical cables. The mode group 3 includes the 5th and 6th modes of the tensegrity column, which are the 1st bending modes of its horizontal cables. The mode group 4 includes the 7th through 12th modes of the tensegrity column, which are the 2nd bending modes of its vertical cables. The mode group 5 includes the 13th through 15th modes of the tensegrity column, which are the 2nd bending modes of its horizontal cables.

3.3 Discussion

A MAC value between mode shapes of two modes of a structure can be used to evaluate their correlation [36], which can be defined by

$$MAC(\{\varphi_r\},\{\varphi_s\}) = \frac{|\{\varphi_r\}^{\mathrm{T}}\{\varphi_s\}|^2}{(\{\varphi_r\}^{\mathrm{T}}\{\varphi_r\})(\{\varphi_s\}^{\mathrm{T}}\{\varphi_s\})} \times 100\% \quad (1)$$

where φ_r and φ_s represent modal vectors of the r^{th} and s^{th} modes of the structure, respectively, and the superscript T denotes the

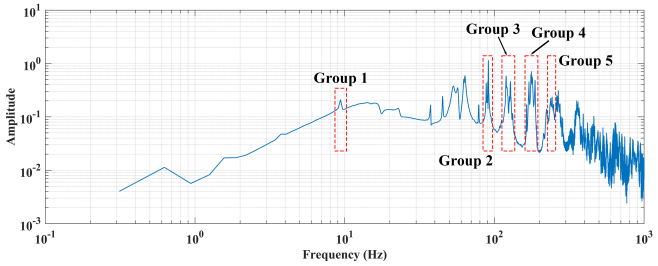

FIGURE 6: Log-log plot of the average FRF for 155 measurement points on the tensegrity column, where the first 15 elastic modes were identified, which were classified into five groups based on their mode types and marked by boxes in red dashed lines

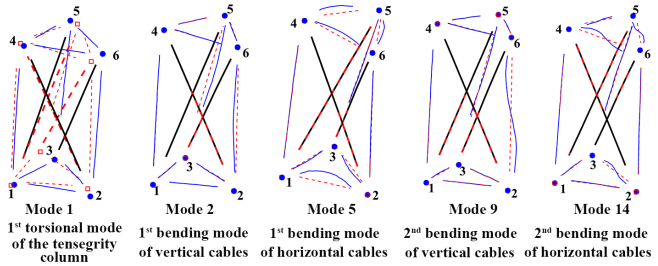

FIGURE 7: Experimental mode shapes and descriptions of five modes of the tensegrity column selected to represent each group

matrix transpose. A MAC value close to 100% indicates a high correlation between the two modes, while a value close to 0 indicates a low correlation. In this work, MAC values are obtained for the first 15 modes of the tensegrity column, forming a matrix shown in Fig. 8, which are also referred to as AutoMAC values. Horizontal and vertical axes of the matrix show natural frequencies of the first 15 modes, and boxes with red dashed lines are used to mark mode groups. The color (or darkness) bar on the right side of the figure indicates that darker colors (heavy darkness) denote higher correlation, while lighter colors (or darkness) denote lower correlation.

One can see that the MAC matrix is symmetrical and its diagonal values are all 100%, as φ_r and φ_s of Eq. (1) are from the same mode in these cases. This satisfies features of AutoMAC values proposed in Ref. [36]. Off-diagonal values of the MAC matrix for mode shapes from different mode groups are less than 10%, indicating that mode shapes from different mode groups are almost uncorrelated. However, a few off-diagonal values of the MAC matrix for mode shapes from the same mode group are around 30%-60%. For example, the MAC value for modes 3 and 4 from the mode group 2 is 35%, whose natural frequencies are 90.3 Hz and 91.3 Hz, respectively. Another instance is the MAC value for modes 7 and 10 from the mode group 4, which of 66%, with their natural frequencies being 170.3 Hz and 177.5 Hz, respectively. One possible reason for non-zero off-diagonal values of the MAC matrix, as proposed in Ref. [36], is that the number of measurement points is not sufficiently large to represent degrees of freedom of the actual structure. By considering the complex 3D shape of the tensegrity column in this work and the fact that relatively high MAC values are found within groups

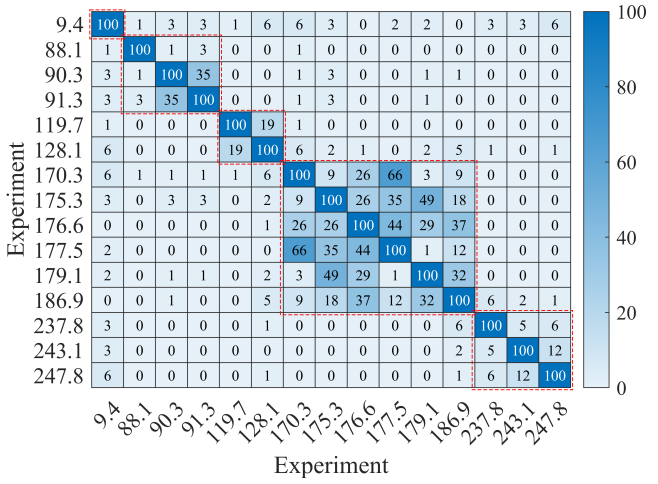

FIGURE 8: AutoMAC matrix of the first 15 experimental mode shapes of the tensegrity column, where boxes with red dashed lines are used to mark mode groups

instead of between groups, MAC values for 3D components of mode shapes are calculated. This exploration aims to identify another possible reason for relatively large off-diagonal values in the MAC matrix. In the 3D MAC value calculation, the modal vector φ in 1 can be replaced by φ_x, φ_y, and φ_z, representing modal vector components along three axes of the global coordinate system shown in Fig. 3. MAC values between modes 3 and 4 from the mode group 2 using their modal vectors along the x-axis of the global coordinate system, those between modes 7 and 10 from the mode group 4 along x-axis, and those between modes 8 and 11 from the mode group 4 along y-axis are shown in Figs. 9a, 9b, and 9c, respectively. Off-diagonal MAC values in these cases are close to 100%, indicating that these compared mode shapes are highly correlated along one axis, potentially contributing to the overall increase in MAC values in these cases. A further comparison is conducted on mode shapes of modes 3 and 4 from different views, as shown in Fig. 10. From Figs. 10a and 10b, which show mode shapes of the tensegrity column from the xz view for modes 3 and 4, respectively, one can see that they are close to each other in both amplitude and phase, corresponding to the MAC value of 96% in Fig. 9a. However, when examining mode shapes from the yz view as shown in Figs. 10c and 10d, differences become apparent. For instance, mode shapes of the two modes of the cable 1_4 have different amplitudes and phases, while those of cables 2_6 and 3_5 have slightly different amplitudes but same phases. In summary, it is significant to obtain 3D vibrations and mode shapes of a structure with a complex 3D shape, such as the tensegrity column in this work, for distinguishing its modes, which can be indistinguishable from 1D vibration and mode shapes.

It can be noted from Fig. 6 that peaks in the FRF of the tensegrity column between mode groups 1 and 2 do not correspond to actual modes. As an example, the deflection shape of the tensegrity column at the frequency 63.4 Hz is shown in Fig. 11. The left part in Fig. 6 shows its overall deflection shape, while the right part shows the deflection shape of nodal points and cables of the bottom plane from the xy view. One can see that

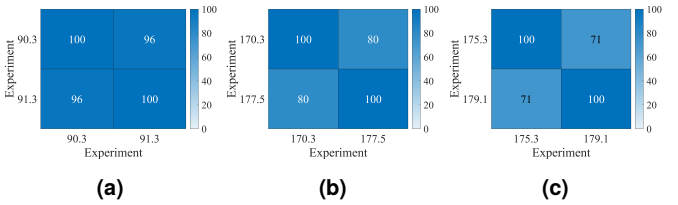

FIGURE 9: (a) MAC values between modes 3 and 4 using their modal vectors along the x-axis of the global coordinate system, (b) MAC values between modes 7 and 10 using their modal vectors along the x-axis, and (c) MAC values between modes 8 and 11 using their modal vectors along the y-axis

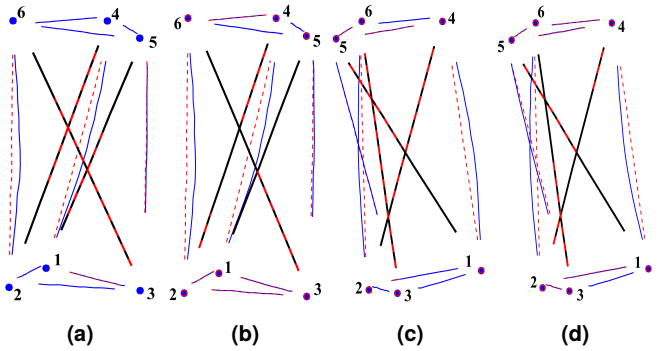

FIGURE 10: Mode shapes of the tensegrity column of its (a) mode 3 from the xz view, (b) mode 4 from the xz view, (c) mode 3 in the yz view, and (d) mode 4 from the yz view

cable and strut members are in rigid-body status, whose deflections are much larger than displacements of nodal points. Significant discontinuities at nodal points make the deflection shape excluded from real mode shapes, as shown in Fig. 11. Peaks in the FRF corresponding to non-mode deflection shapes are potentially caused by phase differences between different structural members induced by measurement noise.

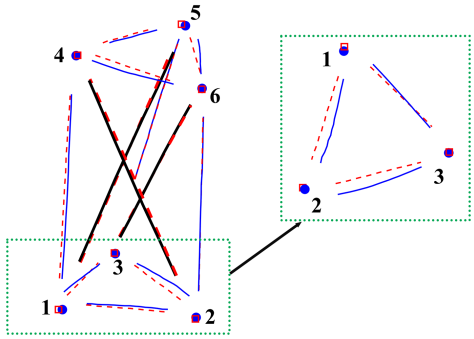

FIGURE 11: Deflection shape of the tensegrity column corresponding to the frequency 63.4 Hz in its FRF, which serves as an example of unreal mode shapes

4. COMPARISON BETWEEN EXPERIMENTAL AND NUMERICAL MODAL PARAMETERS OF THE TENSEGRITY COLUMN

4.1 Numerical modeling and dynamic analysis methods of the tensegrity column

Modeling of the tensegrity structure in this work follows five assumptions [13, 14]: (1) The modeled tensegrity structure only consists of cable and strut members that are connected through frictionless pin-joints. (2) A level of self-stress is required to stiffen the structure and avoid slacking cable members. (3) Mass moments of inertia of cable and strut members along their axial directions are neglected. (4) Only axial forces are transmitted in members. Bar members can sustain both tension and compression forces, and cable members can only sustain tension forces. Bending of cable and strut members, and buckling of strut members do not occur. (5) Materials of cable and strut members are elastic and homogeneous. Cross-sectional areas are constant along lengths of cable and strut members. Thus, mass distributions of cable and strut members are uniform along their axial directions.

The force density method with member grouping is used in this work to determine the initial equilibrium configuration of the tensegrity column. Force equilibrium equations for its i-th node can be written as a system of nonlinear algebraic equations in terms of nodal coordinates (x_i, y_i, y_i):

$$\begin{aligned} \sum_j \frac{T_{ij}}{L_{ij}}(x_i - x_j) = 0 \\ \sum_j \frac{T_{ij}}{L_{ij}}(y_i - y_j) = 0 \\ \sum_j \frac{T_{ij}}{L_{ij}}(z_i - z_j) = 0 \end{aligned} \tag{2}$$

where j denotes the number of a nodal point that is connected to the i-th nodal point via a structural member, T_{ij} denotes the internal force of the structural member, and L_{ij} denotes the length of the structural member. The force density q of a structural member of the tensegrity column that connects the i-th nodal point and the j-th nodal point is defined as

$$q_{ij} = \frac{T_{ij}}{L_{ij}} \tag{3}$$

Eq. 2 then becomes

$$\begin{aligned} \sum_j q_{ij}(x_i - x_j) = 0 \\ \sum_j q_{ij}(y_i - y_j) = 0 \\ \sum_j q_{ij}(z_i - z_j) = 0 \end{aligned} \tag{4}$$

It can also be written in the following matrix form:

$$\begin{aligned} D\mathbf{x} = 0 \\ D\mathbf{y} = 0 \\ D\mathbf{z} = 0 \end{aligned} \tag{5}$$

where the matrix $D = C^{\mathrm{T}}QC$, in which Q is a diagonal matrix containing force densities and C is the branch node matrix, and $\mathbf{x}$, $\mathbf{y}$, and $\mathbf{z}$ are coordinate vectors. For each member j that connects nodes i and k, the matrix C is defined as

$$C = \begin{cases} +1 & \text{for } i(j) = 1 \\ -1 & \text{for } k(j) = 1 \\ 0 & \text{otherwise} \end{cases} \tag{6}$$

For a 3D tensegrity structure, achieving super-stability necessitates adherence to two pivotal criteria, as expounded in Ref. [37]. First, coordinate vectors of the structure must be linearly independent. Second, the structure must satisfy the non-degeneracy condition articulated as $d^* \geq d + 1$, where d^* denotes nullity of the matrix D, and d represents the dimensional space, set at $d = 3$ for a 3D tensegrity structure. Thus, selection of force densities is conducted through an iterative process. This iterative approach is strategically designed, thereby ensuring that both linear independence of coordinate vectors and the non-degeneracy condition are simultaneously satisfied.

In this work, structural members, comprising both cables and struts, are systematically classified into three distinct sets: set one consists of three struts 1_5, 2_4, and 3_6; set two consists of six horizontal cables 1_2, 2_3, 3_1, 4_5, 5_6, and 6_4 placed at the top and bottom of the tensegrity column; and set three consists of three vertical cables 1_4, 2_6, and 3_5. Force densities assigned to structural members within same predefined groups are the same, with q_1, q_2, and q_3 being force densities of sets one, two, and three, respectively. This approach is in adherence to unilateral property criteria, stipulating that strut members must be subjected to compression, whereas cable members should sustain tension. Consequently, force densities for strut members are designated as negative values to reflect their compressive forces, while those for cable members are assigned positive values, indicative of tensile forces.

Subsequently, the CSD method [26] is used to conduct a dynamic analysis on the numerical model, determining its theoretical modal parameters. Consider a strut member that connects two nodal points of a tensegrity structure in a 3D global Cartesian coordinate system. Global Cartesian coordinates of its two nodal points are given as $X_0 = [x_0, y_0, z_0]^{\mathrm{T}}$ and $X_1 = [x_1, y_1, z_1]^{\mathrm{T}}$, respectively. The longitudinal direction of the strut member can be expressed by a position vector $\mathbf{R}_s = X_1 - X_0$, and an independent natural spatial variable $\xi \in [0, 1]$ is used to describe its internal position. The position $u_s(\xi, t)$ of a differential element of a strut member at the position ξ can be expressed as [38–40]

$$\begin{aligned} u_s(\xi, t) &= \tilde{u}_s(\xi, t) + \hat{u}_s(\xi, t) \\ &= \sum_{m=1}^{N_s} q_m^s \sin(m\pi\xi)\mathbf{r}_s + [(1-\xi)X_0 + \xi X_1] \end{aligned} \tag{7}$$

The internal term $\tilde{u}_s$ is defined to satisfy only simple homogeneous boundary conditions, where N_s is a positive integer that controls the complexity and accuracy of the method, and q_m^s are generalized coordinates that describe the internal longitudinal displacement of the strut member. The unit vector $\mathbf{r}_s = \mathbf{R}_s/L_s$ represents the longitudinal direction of the strut member, where

L_s is the deformed member length subjected to a level of self-stress [41]. The boundary-induced term $\hat{u}_s$ is defined to satisfy boundary conditions, which are positions of nodal points in dynamic modeling of the tensegrity structure. The velocity $\dot{u}_s$ of the differential element of the strut member can be obtained by taking the time derivative of Eq. 7. Since the internal displacement described by generalized coordinates is usually significantly small than the deformed length of the bar member, it can be assumed that $q_m^s/L_s \approx 0$. Therefore, terms in the velocity $\dot{u}_s$ associated with q_m^s/L_s vanish and the velocity $\dot{u}_s$ becomes

$$\dot{u}_s(\xi,t) = \sum_{m=1}^{N_s} \dot{q}_m^s \sin(m\pi\xi)\mathbf{r}_s + (1-\xi)\dot{X}_0 + \xi\dot{X}_1 \tag{8}$$

Similarly, for a cable member between nodes X_0 and X_1 of the tensegrity structure in the 3D global Cartesian coordinate system, its position $u_c(\xi,t)$ can also be expressed as a summation of the internal term and the boundary-induced term:

$$u_c(\xi,t) = \tilde{u}_c(\xi,t) + \hat{u}_c(\xi,t) \tag{9}$$

where the boundary-induced term $\hat{u}_c$ has the same form as that of the strut member in Eq. 7, and the internal term $\tilde{u}_c$ differs from that in Eq. 7 with an extra transverse term $\tilde{u}_c^t$ besides the longitudinal term $\tilde{u}_c^l$, since the cable member is modeled as a taut string with both longitudinal and transverse displacements, i.e.,

$$\begin{aligned}\tilde{u}_c =& \tilde{u}_c^l + \tilde{u}_c^t = \sum_{m=1}^{N_l} q_m^l \sin(m\pi\xi)\mathbf{r}_c + \sum_{n=1}^{N_t} q_n^{t_1} \sin(n\pi\xi)\mathbf{w}_1 \\ &+ \sum_{n=1}^{N_t} q_n^{t_2} \sin(n\pi\xi)\mathbf{w}_2\end{aligned} \tag{10}$$

where N_l and N_t are positive integers that control the complexity and accuracy of the method; q_m^l, $q_n^{t_1}$, and $q_n^{t_2}$ are generalized coordinates that describe the internal displacement of the cable member along its longitudinal and two transverse directions, respectively; and unit vectors $\mathbf{r}_c = \mathbf{R}_c/L_c$, $\mathbf{w}_1 = \mathbf{W}_1/L_1$, and $\mathbf{w}_2 = \mathbf{W}_2/L_2$ represent three directions of the cable member, respectively, in which the vector $\mathbf{R}_c = X_1 - X_0$, the vector $\mathbf{W}_1$ can be defined as one of the three possible forms: $[y_0-y_1, x_1-x_0, 0]$, $[z_0-z_1, 0, x_1-x_0]$, and $[0, z_0-z_1, y_1-y_0]$, and the vector $\mathbf{W}_2$ can be obtained by $\mathbf{R}_c \times \mathbf{W}_1$. Scalars L_1 and L_2 are magnitudes of vectors $\mathbf{W}_1$ and $\mathbf{W}_2$, respectively.

The velocity $\dot{u}_c$ of a differential element of the cable member can be obtained by taking the time derivative of Eq. (9). Since the internal displacement described by generalized coordinates is usually significantly smaller than the deformed length of the cable member, it can be assumed that $q_m^l/L_c \approx 0$, $q_n^{t_1}/L_1 \approx 0$, and $q_n^{t_2}/L_2 \approx 0$. Therefore, terms in the velocity $\dot{u}_c$ associated with q_i^l/L_c, $q_j^{t_1}/L_1$, and $q_j^{t_2}/L_2$ vanish, and the velocity $\dot{u}_c$ becomes

$$\begin{aligned}\dot{u}_c(\xi,t) =& \sum_{m=1}^{N_l} \dot{q}_m^l \sin(m\pi\xi)\mathbf{r}_c + \sum_{n=1}^{N_t} [\dot{q}_n^{t_1} \sin(n\pi\xi)\mathbf{w}_1 \\ &+ \dot{q}_n^{t_2} \sin(n\pi\xi)\mathbf{w}_2] + (1-\xi)\dot{X}_0 + \xi\dot{X}_1\end{aligned} \tag{11}$$

Kinetic and potential energies of cable and strut members can then be easily obtained by using the position and velocity in Eqs. 7-11 in the global Cartesian coordinate system. Finally, nonlinear equations of motion of cable and strut members can be obtained by Lagrange's equations. Nonlinear equations of motion of cable and strut members can be linearized at an equilibrium configuration of the tensegrity structure for vibration analysis. A dynamic model of the entire tensegrity structure can be assembled in a straightforward way by using common nodal coordinates of structural members, without a local-to-global coordinate transformation. Theoretical parameters of the tensegrity structure from vibration analysis can then be compared to those obtained experimentally, following the flowchart shown in Fig. 12.

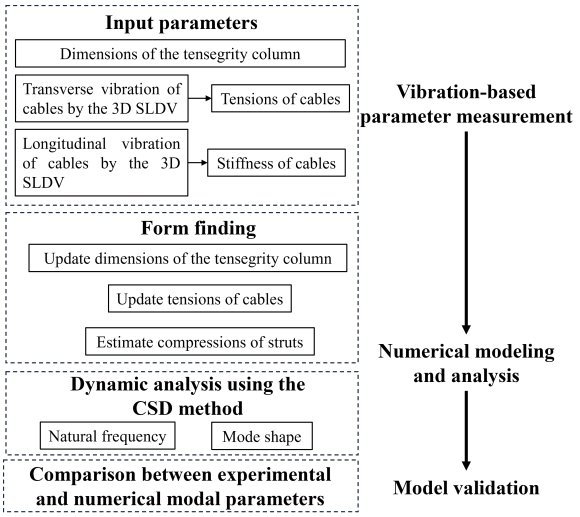

FIGURE 12: Flowchart of numerical modeling and dynamic analysis methods of the tensegrity column

4.2 Cable tension and axial stiffness estimation using the 3D SLDV

The purpose of this section is to determine tensions and axial stiffnesses of cable members of the tensegrity column through modal analysis, referred to as vibration-based parameter measurement in Fig. 12. The k^{th} transverse natural frequency ω_k^{tr} of a uniform string with fixed-fixed boundary conditions can be expressed as [42]

$$\omega_k^{\text{tr}} = \beta_k\sqrt{\frac{T}{\rho}} = k\frac{\pi}{L}\sqrt{\frac{T}{\rho}} = k\pi\sqrt{\frac{T}{\rho L^2}} \tag{12}$$

where $k = 1, 2, \ldots$ represents the order of the transverse natural frequency of the cable, T denotes its tension, ρ denotes its mass per unit length that is 0.074 lb/ft (0.11 kg/m) in this work, and L is its length between two fixed ends. Therefore, the cable tension can be calculated by

$$T = \frac{(\omega_k^{\text{tr}})^2\rho L^2}{k^2\pi^2} = \frac{(2\pi f_k^{\text{tr}})^2\rho L^2}{k^2\pi^2} = \frac{4\rho L^2}{k^2}(f_k^{\text{tr}})^2 \tag{13}$$

where f_k^{tr} is the k-th transverse natural frequency of the cable in Hz, which can be directly obtained from its modal analysis. Corresponding transverse mode shapes can be written as

$$U_k(x) = \sqrt{\frac{2}{\rho L}}\sin\left(k\pi\frac{x}{L}\right) \tag{14}$$

Similarly, the j-th longitudinal natural frequency ω_j^{lo} of a uniform string with fixed-fixed boundary conditions can be expressed as [42]

$$\omega_j^{\text{lo}} = \beta_j \sqrt{\frac{EA}{\rho}} = j\frac{\pi}{L}\sqrt{\frac{EA}{\rho}} = j\pi\sqrt{\frac{EA}{\rho L^2}} \tag{15}$$

where $j = 1, 2, \ldots$ represents the order of the longitudinal natural frequency of the cable, and EA denotes its axial stiffness. Therefore, the cable stiffness can be calculated by

$$EA = \frac{(\omega_j^{\text{lo}})^2 \rho L^2}{j^2\pi^2} = \frac{(2\pi f_j^{\text{lo}})^2 \rho L^2}{j^2\pi^2} = \frac{4\rho L^2}{j^2}(f_j^{\text{lo}})^2 \tag{16}$$

where f_j^{lo} is the longitudinal natural frequency of the cable in Hz, which can be directly obtained from its modal analysis. Corresponding longitudinal mode shapes can be written as

$$U_j(x) = \sqrt{\frac{2}{\rho L}} \sin\left(j\pi\frac{x}{L}\right) \tag{17}$$

The experimental setup for measuring tensions and axial stiffnesses of cable members is shown in Fig. 13. A novel clamping device was designed, which consists of two optical posts and machined clamps, to clamp a cable member at two positions to simulate fixed boundaries. The detailed structure of the clamp is zoomed in and displayed on the right side of Fig. 13. Two thumb screws marked by red arrows were used to fix the cable at one position, ensuring sufficient clearance between the cable and the clamp to avoid potential error from contact. Additionally, the tensegrity column was placed on three foam bases via its three nodes, ensuring that the measured cable remained horizontal and parallel to the optical table. Distances between two clamps and the table were adjusted to be equal to avoid any additional tension induced by bending of the measured cable.

The procedure for determining the tension of the cable 1_4 is exemplified in this section and shown in Fig. 14. A pull-release method was first used to provide an initial excitation to the measured cable. Free vibration responses of multiple points on the cable, as shown in Fig. 14a, were measured to obtain its natural frequencies via the fast Fourier transform (FFT), as shown in Fig. 14b. One can see that responses of different points in the frequency domain align with each other, indicating the rapidity and effectiveness of the pull-release method in obtaining f_k^{tr}, which can be used to calculate T via Eq. 13. However, mode shapes of the cable could not be obtained from free vibration response analysis due to absence of input excitation information to build the FRF of the entire cable. An additional modal analysis method, using a shaker to excite the measured cable, was conducted to obtain both its natural frequencies and mode shapes. As shown in Fig. 13, the shaker was attached to the left fixed end of the measured cable, and a periodic chip with a frequency range of 0 to 500 Hz was used for excitation. Identified natural frequencies and mode shapes of the cable from the shaker test are shown in Figs. 14c and 14d, respectively. One can see that natural frequencies from two test methods are in good agreement, with a maximum difference of 0.26%. Additionally, the first three mode shapes identified from the shaker test align with theoretical results derived from Eq. 14. The right clamp was then repositioned to another location corresponding to a reduced L after finishing the above free vibration test and shaker test, enabling execution of another set of tests to validate the calculated cable tension. Calculated cable tensions of the cable 1_4, obtained from two methods with two different lengths, are listed in Table 3. Tensions of the cable 1_4 measured in different conditions have differences less than 0.5%, validating the accuracy of the cable tension measurement method used in this work. For measuring longitudinal vibrations and obtaining EAs of cable members using Eq. 16, the shaker was rotated by 90 degrees from the position shown in Fig. 13, i.e., aligning it parallel to the measured cable. Results of measured axial stiffnesses of cable members in this work are listed in Table 4. The difference between EAs from two tests with different lengths is approximately 0.6%. Note that the pull-release method was not used for longitudinal vibration measurement, as it is not suitable for exciting longitudinal vibrations with high frequencies.

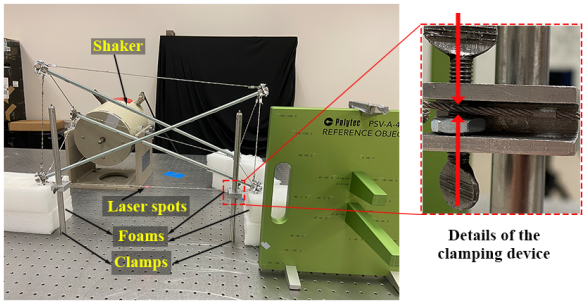

FIGURE 13: Experimental setup for vibration-based cable tension and axial stiffness measurements

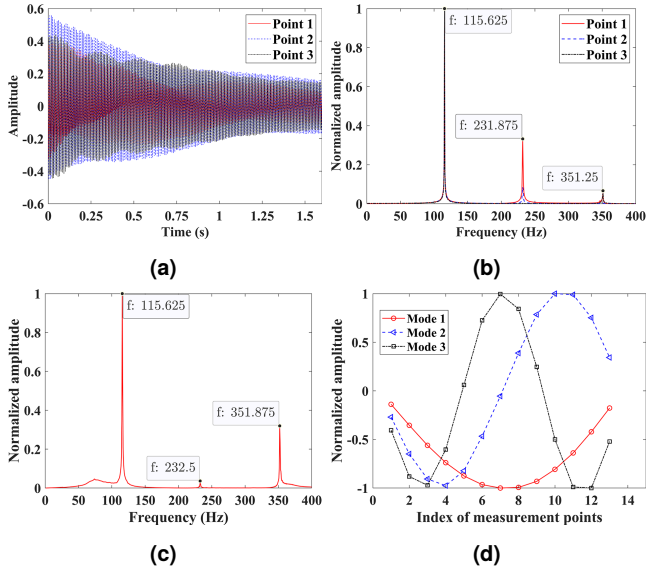

FIGURE 14: Responses of three measurement points on the measured cable 1_4 in (a) the time domain and (b) the frequency domain using the pull-release method, and identified (c) natural frequencies and (d) mode shapes of the cable 1_4 from the shaker test

TABLE 3: Tensions of the cable 1_4 measured by two methods with two different lengths

Test method	L (m)	f_1^{tr} (Hz)	T (N)
Free vibration test	0.422	115.6	104.7
Shaker test	0.422	115.6	104.7
Free vibration test	0.323	151.3	105.1
Shaker test	0.323	151.3	105.1

TABLE 4: Axial stiffnesses of cable members calculated using longitudinal vibration of the cable 1_4

L (m)	f_1^{lo} (Hz)	EA (N)
0.422	4565.4	1.64×10^5
0.323	6015.6	1.63×10^5

4.3 Modal parameters from the numerical model of the tensegrity column

By following the flowchart in Fig. 12 and inputting measured cable tensions and axial stiffnesses into the numerical model of the tensegrity column, its dynamic responses and modal parameters were determined. A total of 37 modes can be extracted and classified into five mode groups, aligning with those from the experiment. Five selected numerical mode shapes are shown in Fig. 15. The mode 1 with a natural frequency of 10.37 Hz corresponds to the 1st torsional mode of the tensegrity column. Modes 2 through 7 with natural frequencies ranging from 97.61 Hz to 98.82 Hz correspond to the 1st bending modes of vertical cables. Modes 8 through 19 with natural frequencies ranging from 102.43 Hz to 104.53 Hz correspond to the 1st bending modes of horizontal cables. Modes 20 through 25 with natural frequencies ranging from 195.15 Hz to 196.01 Hz correspond to the 2nd bending modes of vertical cables. Modes 26 through 37 with natural frequencies ranging from 204.62 Hz to 207.60 Hz correspond to the 2nd bending modes of horizontal cables. Observed misalignment in numbers of identified modes between the numerical model and experiment can be attributed to the fact that intervals between natural frequencies in the same mode group from the numerical model are considerably smaller than the frequency resolution of the experiment. For instance, while two modes were identified in the mode group 3 from the experiment, the numerical model has 12 modes within the same group. Accordingly, the frequency resolution of the experiment was 0.31 Hz, whereas the average value of intervals between natural frequencies of modes in the mode group 3 from the numerical model was 0.19 Hz.

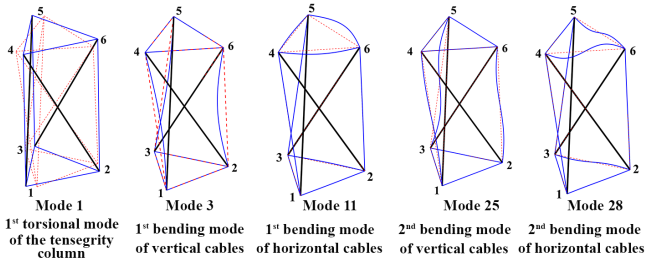

FIGURE 15: Numerical mode shapes and descriptions of five modes of the tensegrity column selected to represent each group

MAC values between mode shapes of the tensegrity column from the experiment and those from its numerical model were calculated using Eq. 1, and those larger than 78% were used to identify mode pairs between experimental and numerical mode shapes. Results shown in Fig. 16a indicate identification of one mode pair from individual mode groups 1, 2, and 3, two mode pairs from the mode group 4, and no mode pair from the group 5. Percentage differences between natural frequencies of paired modes are calculated by using numerical ones as references and less than 15%, as shown in Fig. 16b. Differences between experimental and numerical modal parameters are potentially from misalignment between the numerical model and the actual structure at nodal points, which can lead to differences between their cable lengths.

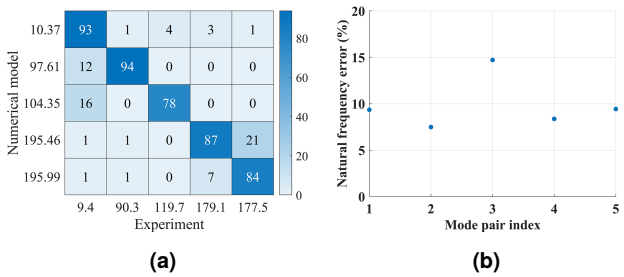

FIGURE 16: (a) MAC values between experimental and numerical mode shapes and (b) differences between experimental and numerical natural frequencies of paired modes

5. CONCLUSIONS

This work proposes a non-contact vibration measurement method using a 3D SLDV for obtaining 3D full-field modal parameters of a tensegrity column. Structural member properties, including cable tensions and axial stiffnesses, are measured using a vibration-based method, which are used to build a numerical model of the tensegrity column for its dynamic analysis. Comparisons between experimental and numerical modal parameters of the tensegrity column are conducted. Some conclusions are listed as follows:

1. With the assistance of a mirror, the FOV of the 3D SLDV is extended, enabling measurements of vibrations at nodal points, as well as cable and strut members of the tensegrity column, to obtain its 3D full-field mode shapes;

2. Natural frequencies and mode shapes of the first 15 elastic modes of the tensegrity column are identified from the experiment and classified into five groups based on their mode types. AutoMAC values of experimental mode shapes show that obtaining 3D vibrations and mode shapes of a structure with a complex 3D shape, such as the tensegrity column in this work, is significant for distinguishing its modes, which can be indistinguishable from 1D vibration and mode shapes;

3. A cable clamping device is designed and used with the 3D SLDV to measure transverse and longitudinal vibrations of cable members for determining accurate cable tensions

and axial stiffnesses, respectively. A form-finding method named the force density method with member grouping is used to build the numerical model of the tensegrity column with initial parameters, including cable tensions and axial stiffnesses, obtained from vibration-based measurements; and

4. The CSD method that avoids the oversimplification problem in traditional methods for dynamic analysis of tensegrity structures is used to obtain modal parameters of the tensegrity column. Numerical modal parameters of the tensegrity column are classified into five mode groups, aligning with those identified from the experiment. Five mode pairs between experimental and numerical results are identified. Differences between natural frequencies of paired modes of the tensegrity column are less than 15%, and MAC values between experimental and numerical mode shapes of paired modes are larger than 78%.

Some future work can be conducted on modifying the numerical model by taking the effect of sizes of nodal points on modal parameters of the tensegrity column into account.

ACKNOWLEDGMENTS

The authors are grateful for the financial support from the National Science Foundation through grant numbers 1763024 and 2104237. They would like to thank capstone design students Alexzander Hunt, Harman Josan, Manu Mathew, and Sean McDonnell for their contributions in designing and assembling the test structure, and Mohammad Riyaz Rehman and Danny Nelson for their contributions in designing the cable clamping device.

REFERENCES

[1] Zhang, Jingyao and Ohsaki, Makoto. *Tensegrity structures*. Vol. 7. Springer (2015).

[2] Ali, Nizar Bel Hadj, Rhode-Barbarigos, Landolf, Albi, Alberto A Pascual and Smith, Ian FC. "Design optimization and dynamic analysis of a tensegrity-based footbridge." *Engineering Structures* Vol. 32 No. 11 (2010): pp. 3650–3659.

[3] Gilewski, Wojciech, Kłosowska, Joanna and Obara, Paulina. "Applications of tensegrity structures in civil engineering." *Procedia Engineering* Vol. 111 (2015): pp. 242–248.

[4] Liedl, Tim, Högberg, Björn, Tytell, Jessica, Ingber, Donald E and Shih, William M. "Self-assembly of three-dimensional prestressed tensegrity structures from DNA." *Nature nanotechnology* Vol. 5 No. 7 (2010): pp. 520–524.

[5] Mirats-Tur, Josep M and Camps, Josep. "A three-DoF actuated robot." *IEEE robotics & automation magazine* Vol. 18 No. 3 (2011): pp. 96–103.

[6] Liu, Yixiang, Bi, Qing, Yue, Xiaoming, Wu, Jiang, Yang, Bin and Li, Yibin. "A review on tensegrity structures-based robots." *Mechanism and Machine Theory* Vol. 168 (2022): p. 104571.

[7] Tibert, AG and Pellegrino, Sergio. "Deployable tensegrity reflectors for small satellites." *Journal of Spacecraft and Rockets* Vol. 39 No. 5 (2002): pp. 701–709.

[8] Yuan, Sichen, Yang, Bingen and Fang, Houfei. "The Projecting Surface Method for improvement of surface accuracy of large deployable mesh reflectors." *Acta Astronautica* Vol. 151 (2018): pp. 678–690.

[9] Yuan, S, Yang, B and Fang, H. "Self-standing truss with hard-point-enhanced large deployable mesh reflectors." *AIAA Journal* Vol. 57 No. 11 (2019): pp. 5014–5026.

[10] Pugh, Anthony. *An introduction to tensegrity*. Univ of California Press (1976).

[11] Tibert, AG and Pellegrino, Sergio. "Review of form-finding methods for tensegrity structures." *International Journal of Space Structures* Vol. 26 No. 3 (2011): pp. 241–255.

[12] Koohestani, K. "Form-finding of tensegrity structures via genetic algorithm." *International Journal of Solids and Structures* Vol. 49 No. 5 (2012): pp. 739–747.

[13] Yuan, Sichen and Zhu, Weidong. "Optimal self-stress determination of tensegrity structures." *Engineering Structures* Vol. 238 (2021): p. 112003.

[14] Yuan, Sichen and Yang, Bingen. "The fixed nodal position method for form finding of high-precision lightweight truss structures." *International journal of Solids and Structures* Vol. 161 (2019): pp. 82–95.

[15] Mirjalili, Seyedali. "The ant lion optimizer." *Advances in engineering software* Vol. 83 (2015): pp. 80–98.

[16] Guest, Simon D. "The stiffness of tensegrity structures." *IMA Journal of Applied Mathematics* Vol. 76 No. 1 (2011): pp. 57–66.

[17] Kan, Ziyun, Peng, Haijun, Chen, Biaoshong, Xie, Xiaohui and Sun, Lining. "Investigation of strut collision in tensegrity statics and dynamics." *International Journal of Solids and Structures* Vol. 167 (2019): pp. 202–219.

[18] Ma, Shuo, Chen, Muhao and Skelton, Robert E. "Tensegrity system dynamics based on finite element method." *Composite Structures* Vol. 280 (2022): p. 114838.

[19] Djouadi, S, Motro, R, Pons, JC and Crosnier, B. "Active control of tensegrity systems." *Journal of Aerospace Engineering* Vol. 11 No. 2 (1998): pp. 37–44.

[20] Yang, Shu and Sultan, Cornel. "LPV state-feedback control of a tensegrity-membrane system." *2016 American Control Conference (ACC)*: pp. 2784–2789. 2016. IEEE.

[21] Wang, Ran, Goyal, Raman, Chakravorty, Suman and Skelton, Robert E. "Model and data based approaches to the control of tensegrity robots." *IEEE Robotics and Automation Letters* Vol. 5 No. 3 (2020): pp. 3846–3853.

[22] Sultan, Cornel and Skelton, Robert. "Deployment of tensegrity structures." *International Journal of Solids and Structures* Vol. 40 No. 18 (2003): pp. 4637–4657.

[23] Kan, Ziyun, Peng, Haijun, Chen, Biaoshong and Zhong, Wanxie. "Nonlinear dynamic and deployment analysis of clustered tensegrity structures using a positional formulation FEM." *Composite Structures* Vol. 187 (2018): pp. 241–258.

[24] Yang, Shu and Sultan, Cornel. "Modeling of tensegrity-membrane systems." *International Journal of Solids and Structures* Vol. 82 (2016): pp. 125–143.

[25] Yang, Shu and Sultan, Cornel. "A comparative study on the dynamics of tensegrity-membrane systems based on multiple models." *International Journal of Solids and Structures* Vol. 113 (2017): pp. 47–69.

[26] Yuan, Sichen and Zhu, Weidong. "A Cartesian spatial discretization method for nonlinear dynamic modeling and vibration analysis of tensegrity structures." *International Journal of Solids and Structures* Vol. 270 (2023): p. 112179.

[27] Bossens, F, De Callafon, RA and Skelton, RE. "Modal Analysis of a Tensegrity Structure–an experimental study." *Dep. Mech. Aerosp. Eng. Dyn. Syst. Control Group, Univ. California, San Diego, USA* (2007).

[28] Małyszko, Leszek and Rutkiewicz, Andrzej. "Response of a Tensegrity Simplex in Experimental Tests of a Modal Hammer at Different Self-Stress Levels." *Applied Sciences* Vol. 10 No. 23 (2020): p. 8733.

[29] Yuan, K and Zhu, WD. "Estimation of modal parameters of a beam under random excitation using a novel 3D continuously scanning laser Doppler vibrometer system and an extended demodulation method." *Mechanical Systems and Signal Processing* Vol. 155 (2021): p. 107606.

[30] Yuan, K and Zhu, WD. "In-plane operating deflection shape measurement of an aluminum plate using a three-dimensional continuously scanning laser Doppler vibrometer system." *Experimental Mechanics* (2022): pp. 1–10.

[31] Yuan, K and Zhu, WD. "A novel general-purpose three-dimensional continuously scanning laser Doppler vibrometer system for full-field vibration measurement of a structure with a curved surface." *Journal of Sound and Vibration* Vol. 540 (2022): p. 117274.

[32] Yuan, K and Zhu, WD. "Identification of modal parameters of a model turbine blade with a curved surface under random excitation with a three-dimensional continuously scanning laser Doppler vibrometer system." *Measurement* Vol. 214 (2023): p. 112759.

[33] Lyu, LF, Yuan, K and Zhu, WD. "A novel demodulation method with a reference signal for operational modal analysis and baseline-free damage detection of a beam under random excitation." *Journal of Sound and Vibration* Vol. 571 (2024): p. 118068.

[34] Yuan, Ke and Zhu, Weidong. "Modeling of welded joints in a pyramidal truss sandwich panel using beam and shell finite elements." *Journal of Vibration and Acoustics* Vol. 143 No. 4 (2021): p. 041002.

[35] Yuan, K and Zhu, WD. "A novel mirror-assisted method for full-Field vibration measurement of a hollow cylinder using a three-dimensional continuously scanning laser Doppler vibrometer system." *Mechanical Systems and Signal Processing* Vol. 216 (2024): p. 111428.

[36] Ewins, D.J. *Modal Testing: Theory, Practice and Application*. Engineering dynamics series, Wiley (2000).

[37] Zhang, JY and Ohsaki, M. "Stability conditions for tensegrity structures." *International journal of solids and structures* Vol. 44 No. 11-12 (2007): pp. 3875–3886.

[38] Zhu, WD and Ren, H. "An accurate spatial discretization and substructure method with application to moving elevator cable-car systems—part I: methodology." *Journal of Vibration and Acoustics* Vol. 135 No. 5 (2013): p. 051036.

[39] Ren, H and Zhu, WD. "An accurate spatial discretization and substructure method with application to moving elevator cable-car systems—part II: application." *Journal of Vibration and Acoustics* Vol. 135 No. 5 (2013): p. 051037.

[40] Wu, K, Zhu, WD and Fan, W. "On a comparative study of an accurate spatial discretization method for one-dimensional continuous systems." *Journal of Sound and Vibration* Vol. 399 (2017): pp. 257–284.

[41] Pellegrino, Sergio and Calladine, Christopher Reuben. "Matrix analysis of statically and kinematically indeterminate frameworks." *International Journal of Solids and Structures* Vol. 22 No. 4 (1986): pp. 409–428.

[42] Meirovitch, L. *Analytical Methods in Vibrations*. Macmillan series in applied mechanics, Macmillan (1967).